

2 *General concepts*

2.1 The general lens

We now consider more realistic lens models, i.e. three dimensional distributions of matter. Even in the case of lensing by galaxy clusters, the physical size of the lens is generally much smaller than the distances between observer, lens and source. The deflection therefore arises along a very short section of the light path. This justifies the usage of the *thin screen approximation* (see Fig. (2.1)): the lens is approximated by a planar distribution of matter, the lens plane. Even the sources are assumed to lie on a plane, called the source plane.

Within this approximation, the lensing matter distribution is fully described by its surface density,

$$\Sigma(\vec{\xi}) = \int \rho(\vec{\xi}, z) dz, \quad (2.1)$$

where $\vec{\xi}$ is a two-dimensional vector on the lens plane and ρ is the three-dimensional density.

As long as the thin screen approximation holds, the total deflection angle is obtained by summing the contribution of all the mass elements $\Sigma(\vec{\xi})d^2\xi$:

$$\vec{\alpha}(\vec{\xi}) = \frac{4G}{c^2} \int \frac{(\vec{\xi} - \vec{\xi}')\Sigma(\vec{\xi}')}{|\vec{\xi} - \vec{\xi}'|^2} d^2\xi'. \quad (2.2)$$

2.2 Lens equation

In Fig. (2.1) we sketch a typical gravitational lens system. A mass concentration is placed at redshift z_L , corresponding to an angular diameter distance D_L . This lens deflects the light rays coming from a source at redshift z_S (or angular distance D_S).

Remark:

It is not guaranteed that the relation between physical size, distance and angular size can be written as [physical size] = [angular size] · [distance] if space is curved. It is however possible to define distances in curved spacetime such that this relation from Euclidean space holds. Then, however, distances are not additive, such that $D_L + D_{LS} \neq D_S$.

We first define an optical axis, indicated by the dashed line, perpendicular to the lens and source planes and passing through the observer. Then we measure the angular positions on the lens and on the source planes with respect to this reference direction.

Consider a source at the angular position $\vec{\beta}$, which lies on the source plane at a distance $\vec{\eta} = \vec{\beta}D_S$ from the optical axis. The deflection angle $\vec{\alpha}$ of the light ray coming from

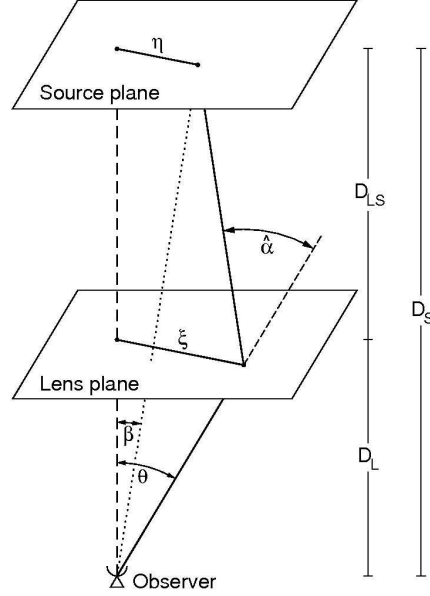


Figure 2.1: Sketch of a typical gravitational lensing system (Figure from Bartelmann & Schneider, 2001).

that source and having an impact parameter $\vec{\xi} = \vec{\theta}D_L$ on the lens plane is given by Eq. (1.36). Due to the deflection, the observer receives the light coming from the source as if it was emitted at the angular position $\vec{\theta}$.

If $\vec{\theta}$, $\vec{\beta}$ and $\hat{\alpha}$ are small, the true position of the source and its observed position on the sky are related by a very simple relation, obtained by a geometrical construction. This relation is called the *lens equation* and is written as

$$\vec{\theta}D_S = \vec{\beta}D_S + \hat{\alpha}D_{LS}, \quad (2.3)$$

where D_{LS} is the angular diameter distance between lens and source.

Defining the reduced deflection angle

$$\vec{\alpha}(\vec{\theta}) \equiv \frac{D_{LS}}{D_S} \hat{\alpha}(\vec{\theta}), \quad (2.4)$$

from Eq. (2.3), we obtain

$$\vec{\beta} = \vec{\theta} - \vec{\alpha}(\vec{\theta}). \quad (2.5)$$

This equation, called *lens equation* is apparently very simple. All the interesting physics of lensing arises because $\vec{\alpha}$ depends on $\vec{\theta}$.

It is very common and useful to write Eq. (2.3) in dimensionless form. This can be done by defining a length scale ξ_0 on the lens plane and a corresponding length scale $\eta_0 = \xi_0 D_S / D_L$ on the source plane. Then we define the dimensionless vectors

$$\vec{x} \equiv \frac{\vec{\xi}}{\xi_0}; \quad \vec{y} \equiv \frac{\vec{\eta}}{\eta_0}, \quad (2.6)$$

as well as the scaled deflection angle

$$\vec{\alpha}(\vec{x}) = \frac{D_L D_{LS}}{\xi_0 D_S} \hat{\alpha}(\xi_0 \vec{x}). \quad (2.7)$$

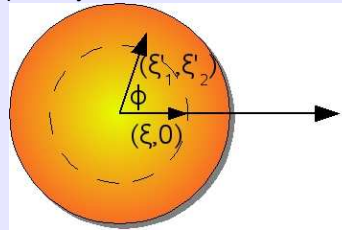
Carrying out some substitutions, Eq. (2.3) can finally be written as

$$\vec{y} = \vec{x} - \vec{\alpha}(\vec{x}) . \quad (2.8)$$

Special case: axially symmetric lenses

In general, the deflection angle is a two-dimensional vector. In the case of axially symmetric lenses we may compute it only in one dimension, since all light rays from the source to the observer must lie in the plane spanned by the center of the lens, the source and the observer. This can be seen explicitly as follows.

We start from Eq. 2.2. Let take the lens center as the origin of the reference frame. By symmetry, we can choose the reference frame such that $\vec{\xi} = (\xi, 0)$, $\xi \geq 0$. In polar coordinates, $\vec{\xi}' = (\xi'_1, \xi'_2) = \xi'(\cos \phi, \sin \phi)$.



Then,

$$\vec{\xi} - \vec{\xi}' = (\xi - \xi' \cos \phi, -\xi' \sin \phi) \quad (2.9)$$

$$\begin{aligned} |\vec{\xi} - \vec{\xi}'|^2 &= \xi^2 + \xi'^2 \cos^2 \phi - 2\xi\xi' \cos \phi + \xi'^2 \sin^2 \phi \\ &= \xi^2 + \xi'^2 - 2\xi\xi' \cos \phi \end{aligned} \quad (2.10)$$

For a symmetric mass distribution $\Sigma(\vec{\xi}) = \Sigma(|\vec{\xi}|)$. The components of the deflection angle are thus

$$\begin{aligned} \hat{\alpha}_1(\vec{\xi}) &= \frac{4G}{c^2} \int_0^\infty d\xi' \xi' \Sigma(\xi') \int_0^{2\pi} d\phi \frac{\xi - \xi' \cos \phi}{\xi^2 + \xi'^2 - 2\xi\xi' \cos \phi} \\ \hat{\alpha}_2(\vec{\xi}) &= \frac{4G}{c^2} \int_0^\infty d\xi' \xi' \Sigma(\xi') \int_0^{2\pi} d\phi \frac{-\xi' \sin \phi}{\xi^2 + \xi'^2 - 2\xi\xi' \cos \phi} \end{aligned} \quad (2.11)$$

By symmetry, the second component of the deflection angle is zero, therefore $\hat{\alpha}$ is parallel to $\vec{\xi}$. Thus, using the lens equation, we find that also the vector $\vec{\eta}$ must be parallel to $\vec{\xi}$.

For the first component of the deflection angle in Eq. 2.11, the inner integral vanishes for $\xi' > \xi$, while it is $2\pi/\xi$ if $\xi' < \xi$. Then, the deflection angle for an axially symmetric lens is

$$\hat{\alpha}(\xi) = \frac{4G}{c^2} \frac{2\pi \int_0^\xi \Sigma(\xi') \xi' d\xi'}{\xi} = \frac{4GM(\xi)}{c^2 \xi} . \quad (2.12)$$

The formula is similar to that derived for a point mass. The deflection is determined by the mass enclosed by the circle of radius ξ , $M(\xi)$.

2.3 Lensing potential

An extended distribution of matter is characterized by its *effective lensing potential*, obtained by projecting the three-dimensional Newtonian potential on the lens plane and by properly rescaling it:

$$\hat{\Psi}(\vec{\theta}) = \frac{D_{LS}}{D_L D_S} \frac{2}{c^2} \int \Phi(D_L \vec{\theta}, z) dz . \quad (2.13)$$

The dimensionless counterpart of this function is given by

$$\Psi = \frac{D_L^2}{\xi_0^2} \hat{\Psi}. \quad (2.14)$$

This lensing potential satisfies two important properties:

- (1) the gradient of Ψ gives the scaled deflection angle:

$$\vec{\nabla}_x \Psi(\vec{x}) = \vec{\alpha}(\vec{x}). \quad (2.15)$$

Indeed,

$$\vec{\nabla}_x \Psi(\vec{x}) = \xi_0 \vec{\nabla}_\perp \left(\frac{D_{LS} D_L}{\xi_0^2 D_S} \frac{2}{c^2} \int \Phi(\vec{x}, z) dz \right) \quad (2.16)$$

$$= \frac{D_{LS} D_L}{\xi_0 D_S} \frac{2}{c^2} \int \vec{\nabla}_\perp \Phi(\vec{x}, z) dz \quad (2.17)$$

$$= \vec{\alpha}(\vec{x}) \quad (2.18)$$

- (2) the Laplacian of Ψ gives twice the *convergence*:

$$\Delta_x \Psi(\vec{x}) = 2\kappa(\vec{x}). \quad (2.19)$$

This is defined as a dimensionless surface density

$$\kappa(\vec{x}) \equiv \frac{\Sigma(\vec{x})}{\Sigma_{cr}} \quad \text{with} \quad \Sigma_{cr} = \frac{c^2}{4\pi G} \frac{D_S}{D_L D_{LS}}, \quad (2.20)$$

where Σ_{cr} is called the *critical surface density*, a quantity which characterizes the lens system and which is a function of the angular diameter distances of lens and source.

Eq. 2.19 is derived from the Poisson equation,

$$\Delta \Phi = 4\pi G \rho. \quad (2.21)$$

The surface mass density is

$$\Sigma(\vec{\theta}) = \frac{1}{4\pi G} \int_{-\infty}^{+\infty} \Delta \Phi dz \quad (2.22)$$

and

$$\kappa(\vec{\theta}) = \frac{1}{c^2} \frac{D_L D_{LS}}{D_S} \int_{-\infty}^{+\infty} \Delta \Phi dz. \quad (2.23)$$

Let us now introduce a two-dimensional Laplacian

$$\Delta_\theta = \frac{\partial^2}{\partial \theta_1^2} + \frac{\partial^2}{\partial \theta_2^2} = D_L^2 \left(\frac{\partial^2}{\partial \xi_1^2} + \frac{\partial^2}{\partial \xi_2^2} \right) = D_L^2 \left(\Delta - \frac{\partial^2}{\partial z^2} \right), \quad (2.24)$$

which gives

$$\Delta \Phi = \frac{1}{D_L^2} \Delta_\theta \Phi + D_L^2 \frac{\partial^2 \Phi}{\partial z^2}. \quad (2.25)$$

Inserting Eq. 2.25 into Eq. 2.23, we obtain

$$\kappa(\vec{\theta}) = \frac{1}{c^2} \frac{D_{LS}}{D_S D_L} \left[\Delta_\theta \int_{-\infty}^{+\infty} \Phi dz + D_L^2 \int_{-\infty}^{+\infty} \frac{\partial^2 \Phi}{\partial z^2} dz \right]. \quad (2.26)$$

If the lens is gravitationally bound, $\partial\Phi/\partial z = 0$ at its boundaries and the second term on the right hand side vanishes. From Eqs. 2.13 and 2.14, we find

$$\kappa(\theta) = \frac{1}{2} \Delta_\theta \hat{\Psi} = \frac{1}{2} \frac{\xi_0^2}{D_L^2} \Delta_\theta \Psi. \quad (2.27)$$

Since

$$\Delta_\theta = D_L^2 \Delta_\xi = \frac{D_L^2}{\xi_0^2} \Delta_x, \quad (2.28)$$

using adimensional quantities Eq. 2.27 reads

$$\kappa(\vec{x}) = \frac{1}{2} \Delta_x \Psi(\vec{x}) \quad (2.29)$$

Integrating Eq. (2.19), the effective lensing potential can be written in terms of the convergence as

$$\Psi(\vec{x}) = \frac{1}{\pi} \int_{\mathbf{R}^2} \kappa(\vec{x}') \ln |\vec{x} - \vec{x}'| d^2 x', \quad (2.30)$$

from which we obtain that the scaled deflection angle is

$$\vec{\alpha}(\vec{x}) = \frac{1}{\pi} \int_{\mathbf{R}^2} d^2 x' \kappa(\vec{x}') \frac{\vec{x} - \vec{x}'}{|\vec{x} - \vec{x}'|}. \quad (2.31)$$

2.4 Magnification and distortion

One of the main features of gravitational lensing is the distortion which it introduces into the shape of the sources. This is particularly evident when the source has no negligible apparent size. For example, background galaxies can appear as very long arcs in galaxy clusters.

The distortion arises because light bundles are deflected differentially. Ideally the shape of the images can be determined by solving the lens equation for all the points within the extended source. In particular, if the source is much smaller than the angular size on which the physical properties of the lens change, the relation between source and image positions can locally be linearized. In other words, the distortion of images can be described by the Jacobian matrix

$$A \equiv \frac{\partial \vec{y}}{\partial \vec{x}} = \left(\delta_{ij} - \frac{\partial \alpha_i(\vec{x})}{\partial x_j} \right) = \left(\delta_{ij} - \frac{\partial^2 \Psi(\vec{x})}{\partial x_i \partial x_j} \right), \quad (2.32)$$

where x_i indicates the i -component of \vec{x} on the lens plane. Eq. (2.32) shows that the elements of the Jacobian matrix can be written as combinations of the second derivatives of the lensing potential.

For brevity, we will use the shorthand notation

$$\frac{\partial^2 \Psi(\vec{x})}{\partial x_i \partial x_j} \equiv \Psi_{ij}. \quad (2.33)$$

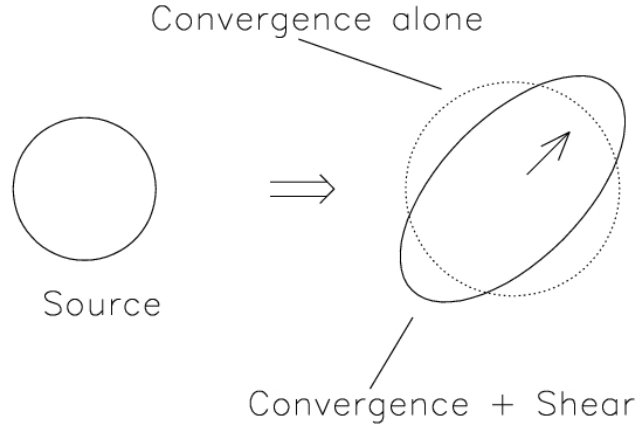


Figure 2.2: Distortion effects due to convergence and shear on a circular source (Figure from Narayan & Bartelmann, 1995).

We can now split off an isotropic part from the Jacobian:

$$\left(A - \frac{1}{2} \text{tr} A \cdot I \right)_{ij} = \delta_{ij} - \Psi_{ij} - \frac{1}{2} (1 - \Psi_{11} + 1 - \Psi_{22}) \delta_{ij} \quad (2.34)$$

$$= -\Psi_{ij} + \frac{1}{2} (\Psi_{11} + \Psi_{22}) \delta_{ij} \quad (2.35)$$

$$= \begin{pmatrix} -\frac{1}{2}(\Psi_{11} - \Psi_{22}) & -\Psi_{12} \\ -\Psi_{12} & \frac{1}{2}(\Psi_{11} - \Psi_{22}) \end{pmatrix}. \quad (2.36)$$

This is manifestly an antisymmetric, trace-free matrix is called the shear matrix. It quantifies the projection of the gravitational tidal field (the gradient of the gravitational force), which describes distortions of background sources.

This allows us to define the pseudo-vector $\vec{\gamma} = (\gamma_1, \gamma_2)$ on the lens plane, whose components are

$$\gamma_1(\vec{x}) = \frac{1}{2} (\Psi_{11} - \Psi_{22}) \quad (2.37)$$

$$\gamma_2(\vec{x}) = \Psi_{12} = \Psi_{21}, \quad (2.38)$$

This is called the *shear*.

The eigenvalues of the shear matrix are

$$\pm \sqrt{\gamma_1^2 + \gamma_2^2} = \pm \gamma. \quad (2.39)$$

Thus, there exists a coordinate rotation by an angle ϕ such that

$$\begin{pmatrix} \gamma_1 & \gamma_2 \\ \gamma_2 & -\gamma_1 \end{pmatrix} = \gamma \begin{pmatrix} \cos 2\phi & \sin 2\phi \\ \sin 2\phi & \cos 2\phi \end{pmatrix} \quad (2.40)$$

Remark:

Note the factor 2 on the angle ϕ , which reminds that the shear component are elements of a 2×2 tensor and not a vector.

The remainder of the Jacobian is

$$\frac{1}{2}\text{tr}A = \left[1 - \frac{1}{2}(\Psi_{11} + \Psi_{22})\right] \delta_{ij} \quad (2.41)$$

$$= \left(1 - \frac{1}{2}\Delta\Psi\right) \delta_{ij} = (1 - \kappa)\delta_{ij}. \quad (2.42)$$

Thus, the Jacobian matrix becomes

$$\begin{aligned} A &= \begin{pmatrix} 1 - \kappa - \gamma_1 & -\gamma_2 \\ -\gamma_2 & 1 - \kappa + \gamma_1 \end{pmatrix} \\ &= (1 - \kappa) \begin{pmatrix} 1 & 0 \\ 0 & 1 \end{pmatrix} - \gamma \begin{pmatrix} \cos 2\phi & \sin 2\phi \\ \sin 2\phi & -\cos 2\phi \end{pmatrix}. \end{aligned} \quad (2.43)$$

The last equation explains the meaning of both convergence and shear. The distortion induced by the convergence is isotropic, i.e. the images are only rescaled by a constant factor in all directions. On the other hand, the shear stretches the intrinsic shape of the source along one privileged direction. For this reason, a circular source, which is small enough compared to the scale of the lens, like that shown in Fig. (2.2) is mapped into an ellipse when κ and γ are both non-zero. The semi-major and -minor axes are

$$a = \frac{r}{1 - \kappa - \gamma}, \quad b = \frac{r}{1 - \kappa + \gamma}, \quad (2.44)$$

where r is the radius of the circular source.

An important consequence of the lensing distortion is the magnification. Through the lens equation, the solid angle element $\delta\beta^2$ (or equivalently the surface element δy^2) is mapped into the solid angle $\delta\theta^2$ (or in the surface element δx^2). Since the Liouville theorem and the absence of emission and absorption of photons in gravitational light deflection ensure the conservation of the source surface brightness, the change of the solid angle under which the source is seen implies that the flux received from a source is magnified (or demagnified).

Given Eq. (2.32), the *magnification* is quantified by the inverse of the determinant of the Jacobian matrix. For this reason, the matrix $M = A^{-1}$ is called the *magnification tensor*. We therefore define

$$\mu \equiv \det M = \frac{1}{\det A} = \frac{1}{(1 - \kappa)^2 - \gamma^2}. \quad (2.45)$$

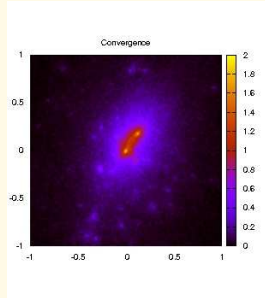
The eigenvalues of the magnification tensor (or the inverse of the eigenvalues of the Jacobian matrix) measure the amplification in the tangential and in the radial direction and are given by

$$\mu_t = \frac{1}{\lambda_t} = \frac{1}{1 - \kappa - \gamma} \quad (2.46)$$

$$\mu_r = \frac{1}{\lambda_r} = \frac{1}{1 - \kappa + \gamma}. \quad (2.47)$$

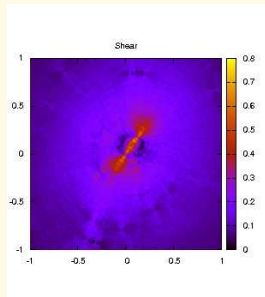
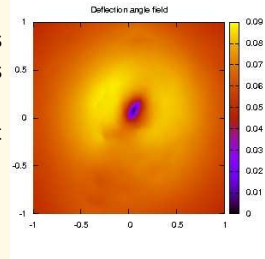
The magnification is ideally infinite where $\lambda_t = 0$ and where $\lambda_r = 0$. These two conditions define two curves in the lens plane, called the *tangential critical line* and the *radial critical line*, respectively. An image forming along the tangential critical line is strongly distorted tangentially to this line. On the other hand, an image forming close to the radial critical line is stretched in the direction perpendicular to the line itself.

Example: Numerically simulated galaxy cluster



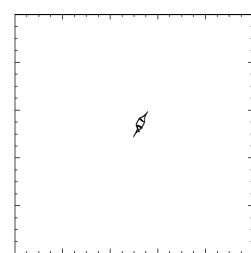
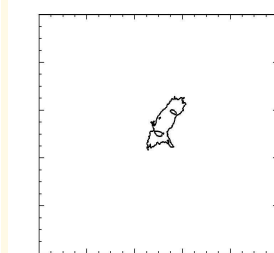
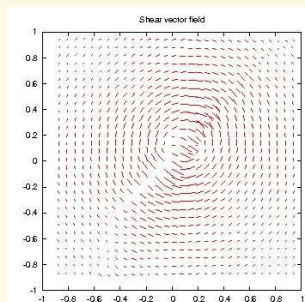
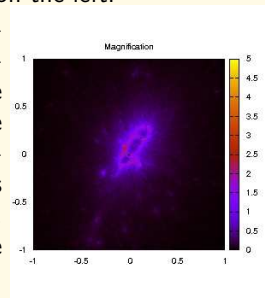
Galaxy clusters are the most massive bound objects in the Universe. They are “young” structures, whose assembling process is still on-going. For this reason they are characterized by an high level of complexity. The luminous matter within them (gas and stars) accounts for $\sim 10\%$ of their mass. The rest is dark matter. Numerical simulations provide the most realistic description of these cosmic structures. N-body and hydrodynamical simulations have been used to simulate the formation and the evolution of systems on different scales. The figure on the left side shows the adimensional surface mass density (or *convergence*) of a cluster-sized dark matter halo simulated at $z \sim 0.3$. The mass of such object is $\sim 10^{15} M_{\odot}$.

Imagine that a bundle of light rays passes through the mass distribution showed above. Each mass element of the lens contributes to deflect the light coming from background sources. Eq.2.2 allows to calculate the deflection angle at each position ξ on the lens plane. The resulting deflection angle field is shown on the right.



The lensing effect can be decomposed into two terms: the isotropic term given by the convergence and the anisotropic term given by the shear γ . This is a pseudo-vector, whose orientation define the direction into which an image is stretched. All around the cluster, the shear tends to be tangential to the lens iso-density contours (see the left panel below). Close to the cluster cores, images can be distorted also towards the cluster center. The intensity of γ determines the amplitude of the distortion. The shear pattern for our numerical cluster is shown on the left.

By distorting them, the lens magnifies the sources. Depending on where the sources are located behind the cluster, the resulting magnification is different. In the Figure on the right shown is the magnification on the lens plane (in logarithmic scale!). It is ideally infinite along the so-called *lens critical lines*. The sources generating images around the critical lines are located along the *caustics*. The critical lines and the caustics are shown in the middle and in the right panels below, respectively.



2.5 Lensing to the second order

In section 2.4, we discussed the effects of lensing at the first order. We briefly mention now some second order effects. Using a Taylor expansion around the origin, the unperturbed coordinates can be linked to the perturbed ones through the following equation

$$y_i \simeq \frac{\partial y_i}{\partial x_j} x_j + \frac{1}{2} \frac{\partial^2 y_i}{\partial x_j \partial x_k} x_j x_k . \quad (2.48)$$

The lensing effect is described at the first order by the Jacobian matrix A . Now, we introduce the tensor

$$D_{ijk} = \frac{\partial^2 y_i}{\partial x_j \partial x_k} = \frac{\partial A_{ij}}{\partial x_k} . \quad (2.49)$$

Then, Eq. 2.48 reads

$$y_i \simeq A_{ij} x_j + \frac{1}{2} D_{ijk} x_j x_k \quad (2.50)$$

By simple algebra, it can be shown that

$$D_{ij1} = \begin{pmatrix} -2\gamma_{1,1} - \gamma_{2,2} & -\gamma_{2,1} \\ -\gamma_{2,1} & -\gamma_{2,2} \end{pmatrix} , \quad (2.51)$$

and

$$D_{ij2} = \begin{pmatrix} -\gamma_{2,1} & -\gamma_{2,2} \\ -\gamma_{2,2} & -2\gamma_{1,2} - \gamma_{2,1} \end{pmatrix} . \quad (2.52)$$

Thus, the second order lensing effect can be expressed in terms of the derivatives of the shear (or in terms of the third derivatives of the potential).

We can construct the complex quantities

$$F = F_1 + iF_2 = (\gamma_{1,1} + \gamma_{2,2}) + i(\gamma_{2,1} - \gamma_{1,2}) \quad (2.53)$$

and

$$G = G_1 + iG_2 = (\gamma_{1,1} - \gamma_{2,2}) + i(\gamma_{2,1} + \gamma_{1,2}) \quad (2.54)$$

which are called *first and second flexion*, respectively. They describe second order distortions of the images of lensed sources.

The flexion is responsible for introducing a curvature and other anisotropic distortions in the images. An illustration of the effects of first and second flexions on the shape of a circular source is shown in Fig. 2.3.

Note that the vector \vec{F} having components F_1 and F_2 is

$$\vec{F} = \vec{\nabla} \kappa . \quad (2.55)$$

Indeed:

$$\gamma_{1,1} = \frac{1}{2} (\Psi_{111} - \Psi_{221}) \quad (2.56)$$

$$\gamma_{2,2} = \Psi_{122} \quad (2.57)$$

$$\gamma_{2,1} = \Psi_{121} \quad (2.58)$$

$$\gamma_{1,2} = \frac{1}{2} (\Psi_{112} - \Psi_{222}) \quad (2.59)$$

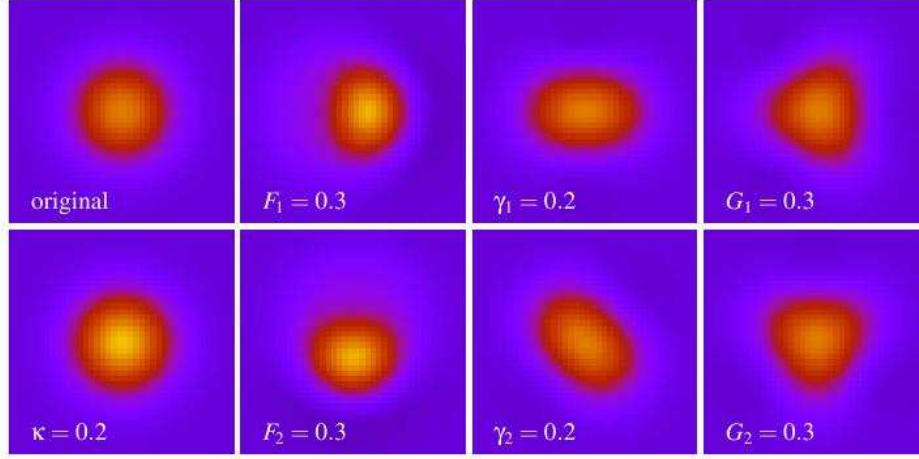


Figure 2.3: First and second order distortions on the image of a circular source. The unlensed source is shown in the top left panel. The convergence simply changes the size (bottom left panel). While the shear deforms the image such that it becomes elliptical (third column of panels from the left), the first and the second flexion introduce curvature and other distortions (second and fourth columns). Courtesy of Peter Melchior.

Therefore:

$$F_1 = \frac{1}{2}(\Psi_{111} - \Psi_{221}) + \Psi_{122} = \frac{1}{2}(\Psi_{111} + \Psi_{221}) = \frac{\partial \kappa}{\partial x_1} \quad (2.60)$$

$$F_2 = \frac{1}{2}(\Psi_{112} - \Psi_{222}) + \Psi_{121} = \frac{1}{2}(\Psi_{112} + \Psi_{222}) = \frac{\partial \kappa}{\partial x_2}. \quad (2.61)$$

This means that the first flexion can be used to obtain the convergence field.

2.6 Occurrence of images

The deflection of light rays causes a delay in the time between the emission of radiation by the source and the signal reception by the observer. This time delay has two components:

$$t = t_{\text{geom}} + t_{\text{grav}} \quad (2.62)$$

The first one has a geometrical reason and is due to the different path length of the deflected light rays compared to the unperturbed ones. This time delay is proportional to the squared angular separation between the intrinsic position of the source and the location of its image. The second one comes from the slowing down of photons traveling through the gravitational field of the lens and is therefore related to the lensing potential. Considering a lens at redshift z_L , the total time delay introduced by gravitational lensing at the position \vec{x} on the lens plane is

$$t(\vec{x}) = \frac{(1 + z_L)}{c} \frac{D_S \xi_0^2}{D_L D_{LS}} \left[\frac{1}{2}(\vec{x} - \vec{y})^2 - \Psi(\vec{x}) \right]. \quad (2.63)$$

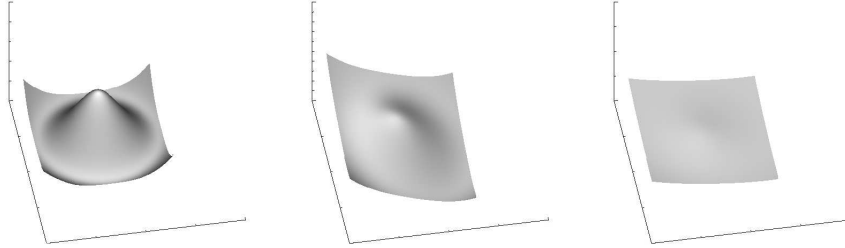


Figure 2.4: Time delay surfaces of an axially symmetric lens for three different source positions. Right panel: source and lens are perfectly aligned along the optical axis; middle panel: the source is no more aligned with the lens. Its projected position on the lens plane is moved along the line $x_1 = x_2$; right panel: the source is moved to an even larger angular distance from the optical axis.

Through the effective lensing potential, the lens equation can be written as

$$(\vec{x} - \vec{y}) - \nabla \Psi(\vec{x}) = \nabla \left[\frac{1}{2}(\vec{x} - \vec{y})^2 - \Psi(\vec{x}) \right] = 0. \quad (2.64)$$

Eqs. (2.63) and (2.64) imply that images satisfy the Fermat Principle, $\nabla t(\vec{x}) = 0$. Images therefore are located at the stationary points of the time delay surface given by Eq. (2.63). The Hessian matrix of this surface is

$$T = \frac{\partial^2 t(\vec{x})}{\partial x_i \partial x_j} \propto (\delta_{ij} - \Psi_{ij}) = A \quad (2.65)$$

We can distinguish between three types of image:

- (1) type I images arise at the minima of the time delay surface, where the eigenvalues of the Hessian matrix are both positive, hence $\det A > 0$ and $\text{tr} A > 0$. Therefore, they have positive magnification;
- (2) type II images arise at the saddle points of the time delay surface, where eigenvalues have opposite signs. Since $\det A < 0$, they have negative magnification. The interpretation of a negative μ is that the parity of the image is flipped compared to the source;
- (3) finally, type III images arise at the maxima of the time delay surface. Here, the eigenvalues are both negative, hence $\det A > 0$ and $\text{tr} A < 0$. These images therefore have positive magnification.

Since the Hessian matrix describes the local curvature of the time delay surface, the smaller is the curvature along one direction at the position where the image forms, the larger is its magnification along the same direction. We display in Fig. (2.4) some examples of the time delay surface for a general axially symmetric lens with core. The density profile of this lens scales with radius as r^{-2} outside the core. The surfaces are plotted for three different source position \vec{y} : in the left panel the source and the lens are perfectly aligned along the optical axis passing through the lens center ($\vec{y} = 0$ and $\vec{x} = 0$); in the middle and right panel, the source is moved far away, increasing its angular distance from the optical axis. In order to better see where the minima and the maxima arise, we show in Fig. (2.5) the profile along the line $x_1 = x_2$ of the same

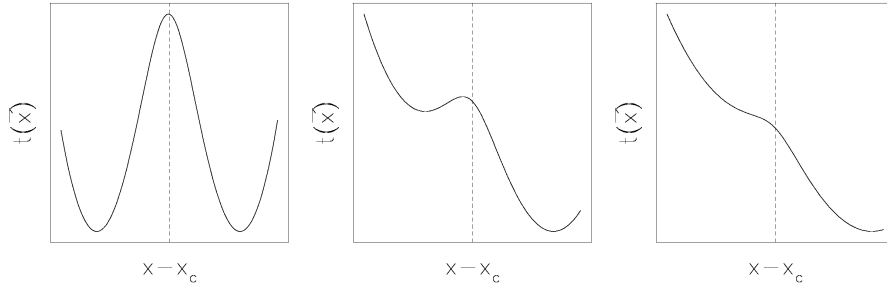


Figure 2.5: Profiles of the time delay surfaces displayed in Fig. (2.4) along the line $x_1 = x_2$.

surfaces. When the source and the lens are perfectly aligned, the minima of the time delay surface are located on a ring and the maximum is at the lens center. The source therefore is mapped to a ring image of type I (the so called *Einstein Ring*) and to a central type III image. This last one is generally demagnified, since the curvature of the time delay surface here is large for density profiles peaked at the lens center.

As the source is moved far away from the optical axis, the time delay surface deforms. In particular, the ring breaks, leading to the formation of a minimum and of a saddle point. Three images therefore arise. In the case displayed in the middle panel of Fig. (2.4), the type I image at the minimum and the type II image at the saddle point are stretched in the tangential direction, since the local curvature of the time delay surface is small in that direction. This explains the formation of tangential arcs in galaxy clusters. However, as the source is moved to even larger angular distances from the optical axis, the saddle point and the maximum move much closer to each other, while the minimum follows the source. The local curvature of the time delay surface in the radial direction becomes smaller between the saddle point and the maximum as they get closer. The images arising at this two points therefore are stretched towards each other. Then a radial image forms. When the saddle point and the maximum point touch, two images disappear and only the image arising at the minimum of the time delay surface remains (see right panels of Fig. (2.4) and Fig. (2.5)).

Here follows a number of other important properties of the time-delay surface:

- the height difference at different images of the surface $t(\vec{x})$ gives the difference in arrival time between these images. This time delay can be measured if the source is variable, and provides one way of potentially measuring the Hubble constant;
- in absence of the lens, the time-delay surface is a parabola which has a single extremum (a minimum); additional extrema have to come in pairs, thus the total number of images must be odd (as we showed earlier by continuously deforming the time-delay surface);
- when two additional images are formed, they must be a maximum and a saddle point; in between them, the curvature changes from negative to positive, thus it is zero between them; remember that $\det A = 0$ is the condition for having a critical point, where the magnification is (formally) infinite. The critical lines thus separate multiple-image pairs; these pairs merge and disappear (as discussed above) at the critical lines. In other words, the critical lines separate regions of different image multiplicities.

Example: Determination of the Hubble Constant

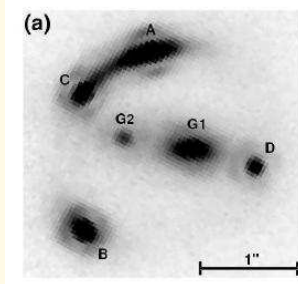
The lens equation is dimensionless, and the positions of images as well as their magnifications are dimensionless numbers. Therefore, information on the image configuration alone does not provide any constraint on the overall scale of the lens geometry or the value of the Hubble constant. Refsdal 1964 realized that the time delay, however, is proportional to the absolute scale of the system and does depend on H_0 .

To see this, we first note that the geometrical time delay is simply proportional to the path lengths of the rays which scale as H_0^{-1} . The gravitational time delay also scales as H_0^{-1} because the linear size of the lens and its mass have this scaling. Therefore for any gravitational lens system, the quantity

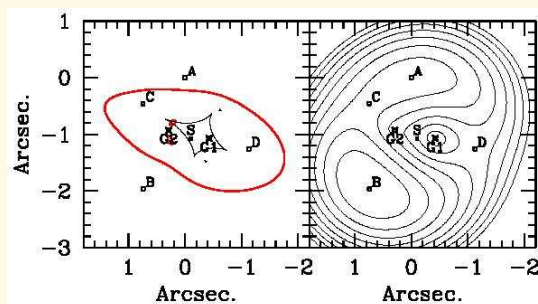
$$H_0 \Delta t$$

depends only on the lens model and the geometry of the system. A good lens model which reproduces the positions and magnifications of the images provides the scaled time delay $H_0 \Delta t$ between the images. Therefore, a measurement of the time delay Δt will yield the Hubble constant H_0 .

As an example, we summarize here the results of Koopmans et al. (2003). They analyse the lens system B1608+656, a quadruply-imaged QSO at redshift $z_S = 1.39$ lensed by two lens galaxies at redshift $z_L = 0.63$ (see Fig. on the right side). For this system very accurate determinations of the time delays between the different images were obtained by Fassnacht et al. (2002), by monitoring the VLA radio fluxes of the four images. Labelling the images from A to D, the time-delays with respect to the image B were found to be $\Delta t_{AB} = 31.5 \pm 1.5$, $\Delta t_{CB} = 36 \pm 1.5$ and $\Delta t_{DB} = 77 \pm 1.5$ (days).



By combining several radio, optical, infrared observations plus some constraints on the dynamics of stars in the main lens galaxy (G1), Koopmans et al. were able to construct a detailed model of the lens system, and to reconstruct the shape of the time-delay surface.



The lens critical lines (in red) and caustics (in black) are shown in the left panel, the contours of constant time-delay on the right. They start at $\Delta t = 0$ at image B and increase in steps of $10h^{-1}$ days. As expected, images B and A correspond to minima of the time-delay surface. Image C and D are located at two saddle points, instead.

Finally, a maximum falls onto the galaxy G1, where no images of the source QSO are seen. For this galaxy, the lens model predicts a very large inner slope of its density profile. Consequently, the local curvature of the time-delay surface is very large. Thus, the image which should form at this position is strongly de-magnified. The light of the lens galaxy also prevents to observe such image. Note that the critical lines pass between the saddle and the minimal points.

Using this lens model, Koopmans et al. estimate the Hubble constant to be $H_0 = 75_{-6}^{+7}$ km s $^{-1}$ Mpc $^{-1}$.

Bibliography

Einstein, A., 1916, *Ann. der Ph.*, **49**, 769

Fassnacht, C. D., Xanthopoulos, E., Koopmans, L. V. E., & Rusin, D., 2002, *ApJ*, **581**, 823

Koopmans, L. V. E., Treu, T., Fassnacht, C. D., Blandford, R. D., & Surpi, G., 2003, *ApJ*, **599**, 70

Refsdal, S., 1964, *MNRAS*, **128**, 307

Shapiro, I. I., 1964, *Phys. Rev. Lett.*, **13**, 789

Soldner, J., 1801, *Berliner Astronomisches Jahrbuch fuer Jahr 1804*, Cambridge University Press

Will, C. M., 1988, *Am. J. Phys.*, **56**, 5